Quantifying the Sensitivity of a Balmer Spectroscopy for Hydrogen Plasma Diagnostics Using a Collisional-Radiative Model

Logan Ramanathan

April 2026

Abstract

A collisional-radiative model for atomic hydrogen is constructed to determine where Balmer-line spectroscopy provides reliable plasma diagnostics. The model tracks 15 energy levels, using rate coefficients from Vriens and Smeets (1980) and oscillator strengths from Johnson (1972), and is validated against the published results of Vinoth et al. (2022) as well as the analytic coronal and Saha-Boltzmann equilibrium limits. Sensitivity maps of the Balmer line ratios Hβ/Hα and Hγ/Hβ reveal that temperature sensitivity is confined to $kT_e \lesssim 5$ eV, while density sensitivity peaks in the collisional-radiative transition region $n_e \sim 10^{11}$–10^{13} cm^{-3}. The model was extended to a time-dependent mode using a BDF integrator, and for oscillating plasma conditions, the steady-state diagnostic prediction was found to break down near $\sim$100 kHz at $n_e = 10^{10}$ cm^{-3}, but only break down near $\sim$1 MHz at $n_e = 10^{15}$ cm^{-3}. Eigenvalue analysis of the rate matrix provides an independent estimate of equilibration timescales that agrees with the full numerical integration, and the time-dependent response exhibits nonlinear amplification effects.

1 Introduction

Measuring electron temperature and density in a plasma is essential for applications ranging from fusion energy research to spacecraft propulsion to industrial processing. Spectroscopy offers a non-invasive approach: by observing the relative brightness of atomic emission lines, one can infer the internal properties of the plasma without inserting physical probes. For hydrogen plasmas, the Balmer series—visible-wavelength photons emitted when atoms decay from excited levels to $n = 2$—is particularly convenient. Hα (656 nm, $n = 3 \to 2$), Hβ (486 nm, $n = 4 \to 2$), and Hγ (434 nm, $n = 5 \to 2$) are all in the visible range and readily measured with standard spectrometers.

The connection between emission line ratios and plasma parameters depends on the regime. At very low electron density, each excited level is populated only by electron-impact excitation from the ground state and depopulated by spontaneous radiative decay. In this coronal limit, line ratios depend on temperature alone. At very high density, collisions are so frequent that they drive all level populations into the Boltzmann distribution, and line ratios again depend only on temperature. Many laboratory and astrophysical plasmas fall between these extremes, in the collisional-radiative regime where both collisional and radiative processes contribute. In this regime, line ratios depend on both T_e and n_e, and a collisional-radiative (CR) model is needed to extract plasma parameters from measured spectra.

The central question of this work is: over what range of electron temperature and density do Balmer line ratios provide reliable, independent constraints on plasma parameters, and where do these diagnostics lose sensitivity? I address this question in two parts. First, I map the steady-state sensitivity of Balmer ratios across the (T_e, n_e) parameter space and identify the regions where each

ratio is a useful diagnostic. Second, I extend the model to time-dependent mode to determine when the steady-state assumption itself breaks down—specifically, how rapidly plasma conditions can change before spectroscopic diagnostics become unreliable. This second question is motivated by the fact that many plasmas of practical interest are not static.

The starting point for this work is the CR model of Vinoth et al. (2022) [2], who computed Balmer line ratios for atomic hydrogen using the rate coefficients of Vriens and Smeets [1] and validated against their experimental measurements. The present work extends their model in three ways. First, three-body recombination is added to the rate equation, enabling validation against the Saha-Boltzmann (LTE) limit and revealing where recombination affects diagnostics at the boundary of Vinoth et al.'s parameter range. Second, the steady-state line ratios are mapped across the full two-dimensional (T_e, n_e) parameter space and their partial derivatives are computed to quantify diagnostic sensitivity. Third, the model is extended to time-dependent mode by integrating the rate equations forward in time with a BDF solver, allowing the determination of how fast plasma conditions can change before steady-state spectroscopic diagnostics become unreliable.

2 Background and Theory

2.1 Hydrogen Atomic Data

The ionization energy of hydrogen level n is $E_n = \mathcal{R}/n^2$ with $\mathcal{R} = 13.6$ eV. The transition energy between levels p and n ($n > p$) is

$$E_{pn} = \mathcal{R}\left(\frac{1}{p^2} - \frac{1}{n^2}\right). \tag{1}$$

Oscillator strengths are computed from the approximation of Johnson (1972) [3]:

$$f_{pn} = \frac{32}{3\sqrt{3}\,\pi}\frac{p}{n^3}x^{-3}g(p,x), \quad x = 1 - \left(\frac{p}{n}\right)^2, \tag{2}$$

where $g(p,x) = g_0(p) + g_1(p)\,x^{-1} + g_2(p)\,x^{-2}$ is the Gaunt factor correction. The oscillator strength quantifies how strongly two levels couple through the electromagnetic field: a large f_{pn} means the atom readily absorbs or emits photons at the corresponding frequency, and also that electron-impact transitions between those levels are relatively efficient.

Einstein A coefficients for spontaneous radiative decay are computed from the oscillator strengths via

$$A_{n\to m} = \frac{6.6703\times10^{15}}{\lambda_{\text{Å}}^2}\frac{g_m}{g_n}f_{mn}, \quad g_n = 2n^2, \tag{3}$$

from the standard relation between Einstein A coefficients and oscillator strengths (see, e.g., Ref. [4]), where $\lambda_{\text{Å}} = 12398.4/E_{mn}$ is the transition wavelength in Ångströms. These were verified against exact quantum mechanical values tabulated by the Ioffe Institute from the formulas of Berestetskii et al. [4]; agreement is better than 0.1% (Table 2).

2.2 Collisional Rate Coefficients

All collisional rate coefficients are computed from the analytical formulas of Vriens and Smeets (1980) [1]. The electron-impact excitation rate coefficient for a transition $p \to n$ ($n > p$) is (their Eq. 17):

$$K_{pn}^{\text{exc}} = \frac{1.6\times10^{-7}\,(kT_e)^{0.5}}{kT_e + \Gamma_{pn}}\exp(-\varepsilon_{pn})\left[A_{pn}\ln\!\left(\frac{0.3\,kT_e}{\mathcal{R}} + \Delta_{pn}\right) + B_{pn}\right], \tag{4}$$

in $\mathrm{cm}^3\,\mathrm{s}^{-1}$, where $\varepsilon_{pn} = E_{pn}/kT_e$. The Bethe coefficients $A_{pn} = (2\mathcal{R}/E_{pn})f_{pn}$ and B_{pn} (Vriens Eqs. 11–13) encode the dipole and non-dipole contributions to the collision, respectively. The auxiliary quantities Δ_{pn} and Γ_{pn} (Eqs. 18–19) prevent unphysical behavior at low and high energies; Γ_{pn} is the only quantity that depends on temperature.

The ionization rate coefficient from level p is (Vriens Eq. 8):

$$K_{pi} = \frac{9.56 \times 10^{-6}\,(kT_e)^{-1.5}\exp(-\varepsilon_{pi})}{\varepsilon_{pi}^{2.33} + 4.38\,\varepsilon_{pi}^{1.72} + 1.32\,\varepsilon_{pi}}. \tag{5}$$

De-excitation rates are obtained from excitation rates through detailed balance, the thermodynamic principle that in equilibrium every forward process is exactly balanced by its reverse:

$$K_{pn}^{\mathrm{deexc}} = \frac{g_n}{g_p}\,K_{np}^{\mathrm{exc}}\,\exp\!\left(\frac{E_{np}}{kT_e}\right), \quad p > n. \tag{6}$$

Three-body recombination—the capture of a free electron into bound level p with a second electron carrying away the excess energy—is obtained from the ionization rate via the Saha equation (Vriens Eq. 9):

$$\alpha_{ip} = \frac{3.17 \times 10^{-27}\,(kT_e)^{-1.5}\,(g_p/g_i)}{\varepsilon_{pi}^{2.33} + 4.38\,\varepsilon_{pi}^{1.72} + 1.32\,\varepsilon_{pi}} \tag{7}$$

in $\mathrm{cm}^6\,\mathrm{s}^{-1}$. The recombination rate per unit volume scales as $n_e^2\alpha_{ip}$, making it significant only at high density.

2.3 Rate Equation

For each excited level i, the population $n(i)$ evolves according to the standard collisional-radiative rate equation [2]:

$$\begin{aligned}\frac{dn(i)}{dt} = &\sum_{k\neq i} n_e\,n(k)\,K_{k\to i} + \sum_{k>i} A_{k\to i}\,n(k) + n_e^2\,\alpha_{ip} \\ &- n_e\,n(i)\sum_{k\neq i} K_{i\to k} - n(i)\sum_{k<i} A_{i\to k} - n_e\,n(i)\,K_{pi}.\end{aligned} \tag{8}$$

The first line contains sources of population for level i: collisional transfers from other levels, radiative cascade from above, and three-body recombination from the continuum. The second line contains the sinks. Collisional transfers out of a level, radiative decay to lower levels, and ionization. The recombination term $n_e^2\alpha_{ip}$ was omitted in the model of Vinoth et al. [2]; this work includes it to enable validation against the LTE limit and to capture its effect at high density. The ground state population is fixed at $n(1) = 1$; all other populations are computed relative to this reference.

In steady state, $dn(i)/dt = 0$ and Eq. 8 becomes a linear system $\mathbf{M}\,\mathbf{n} = \mathbf{s}$, which is solved with standard linear algebra (`numpy.linalg.solve`). The Balmer line intensity from level n is $I_n = A_{n\to 2}\,n(n)$, and diagnostic line ratios are formed as, for example, $\mathrm{H}\beta/\mathrm{H}\alpha = A_{4\to 2}\,n(4)/A_{3\to 2}\,n(3)$.

In the time-dependent mode, $dn(i)/dt \neq 0$ and Eq. 8 is instead integrated forward in time as an ODE system. The plasma conditions $kT_e(t)$ and $n_e(t)$ are functions of time, and the rate matrix $\mathbf{M}$ and source vector $\mathbf{s}$ are recomputed at each timestep. Because the rate equation is integrated forward in time, the populations at time t are determined by the populations at the previous timestep and the rates at the current conditions. If the plasma conditions change on a timescale shorter than the slowest relaxation timescale of the rate matrix, the populations will not have reached the steady-state values corresponding to the current kT_e and n_e before the conditions change again. The Balmer ratios computed from these lagging populations will therefore differ from the ratios that a steady-state model would predict at the same instant.

3 Method

3.1 Code Structure

The model is implemented in Python. The computation process goes through four steps: (1) atomic data—energy levels, oscillator strengths, and Einstein A coefficients, which depend only on quantum numbers; (2) Bethe coefficients A_{pn}, B_{pn}, δ_{pn}, which are derived from the atomic data; (3) rate coefficients for excitation, de-excitation, ionization, and recombination, which depend on kT_e; and (4) the rate matrix assembly and linear solve, which depends on both kT_e and n_e. Each layer was tested independently before integration into the full model.

3.2 Time-Dependent Extension

For the time-dependent model, the same rate matrix is used but the system $dn/dt = \mathbf{M}(t)\,\mathbf{n} - \mathbf{s}(t)$ is integrated forward in time using `scipy.integrate.solve_ivp` with the BDF (backward differentiation formula) method. BDF is required because the system is stiff: radiative decay rates can exceed 10^8 s^{-1} while collisional rates at low density may be orders of magnitude slower. When plasma conditions vary in time, $\mathbf{M}$ and $\mathbf{s}$ are recomputed at each timestep using the prescribed $kT_e(t)$ and $n_e(t)$.

4 Initial Verification and Sanity Checks

4.1 Eigenvalue Analysis

The natural timescales of the system are encoded in the eigenvalues of the rate matrix. A perturbation $\delta\mathbf{n}$ from steady state evolves as

$$\delta\mathbf{n}(t) = \sum_k c_k\,\mathbf{v}_k\,e^{\lambda_k t}, \tag{9}$$

where λ_k and $\mathbf{v}_k$ are eigenvalues and eigenvectors of $\mathbf{M}$. For a stable system all $\lambda_k < 0$, and the relaxation timescale for each mode is $\tau_k = -1/\lambda_k$. The slowest mode (smallest $|\lambda_k|$) determines the overall equilibration time: if the plasma evolves on timescales longer than τ_{slowest}, the steady-state model is valid.

4.2 Physical Validation of Model

Coronal limit. In the low-density limit, collisional de-excitation is negligible and each excited level i is populated only by electron-impact excitation from the ground state and depopulated only by spontaneous radiative decay. Setting $dn(i)/dt = 0$ in this limit gives $n(i) = n_e K_{\text{exc}}(1 \to i)/\sum_j A_{i\to j}$. The predicted Balmer ratio is then

$$\left.\frac{\mathrm{H}\beta}{\mathrm{H}\alpha}\right|_{\text{cor}} = \frac{A_{4\to2}\,K_{\text{exc}}(1\to4)}{A_{3\to2}\,K_{\text{exc}}(1\to3)} \cdot \frac{\sum_j A_{3\to j}}{\sum_j A_{4\to j}}, \tag{10}$$

where n_e cancels out, confirming that the ratio depends only on temperature in this regime. At $kT_e = 10$ eV, this analytic formula gives $\mathrm{H}\beta/\mathrm{H}\alpha = 0.215$, while the full 15-level model at $n_e = 10^8$ cm^{-3} gives 0.223. The 4% difference arises because the full model includes radiative cascade from levels above $n = 4$ feeding additional population into levels 3 and 4, which the two-level coronal formula neglects.

LTE limit. At sufficiently high density, collisions drive the level populations toward the Boltzmann distribution $n(i)/n(1) = (g_i/g_1)\exp(-E_{1i}/kT_e)$, where $g_i = 2i^2$. The Balmer ratio in this limit is determined entirely by the Einstein A coefficients, statistical weights, and the Boltzmann factor:

$$\left.\frac{\mathrm{H}\beta}{\mathrm{H}\alpha}\right|_{\mathrm{LTE}} = \frac{A_{4\to2}}{A_{3\to2}} \cdot \frac{g_4}{g_3} \cdot \exp\left(-\frac{E_{13} - E_{14}}{kT_e}\right) = \frac{A_{4\to2}}{A_{3\to2}} \cdot \frac{16}{9} \cdot \exp\left(-\frac{0.66\ \mathrm{eV}}{kT_e}\right). \tag{11}$$

At $kT_e = 10$ eV, this gives $\mathrm{H}\beta/\mathrm{H}\alpha = 0.3177$. The full model with recombination at $n_e = 10^{21}$ cm^{-3} gives 0.3178—agreement to 0.03%. The excited-state population ratios $n(i)/n(i)_{\mathrm{Boltzmann}}$ are all equal to 2.58, confirming that the excited levels are in thermal equilibrium with each other. The constant offset arises because the ground state population is held fixed at $n(1) = 1$ rather than determined self-consistently by the Saha equation. This affects the overall amounts but not the ratios between excited levels.

Convergence. Balmer ratios change by less than 3% between $N = 10$ and $N = 18$ levels (Table 3), confirming that truncating the model at $N = 15$ does not significantly affect the diagnostic line ratios.

Comparison against Vinoth et al. Line ratios versus n_e at five temperatures (10, 80, 100, 200, 400 eV) were compared visually to the atomic hydrogen results published by Vinoth et al. [2], who built an independent CR model using the same Vriens and Smeets rate coefficients but without recombination. The solid lines in Fig. 1 reproduce their Fig. 1, validating the present implementation.

5 Results

5.1 Steady-state Line Ratios

Figure 1 compares line ratios from the present model to the atomic hydrogen results of Vinoth et al. [2], both without recombination (solid lines, reproducing their model) and with three-body recombination included (dashed lines, the present extension). The solid lines validate the implementation of the Vriens and Smeets rate coefficients against an independent CR model. The dashed lines reveal the effect of recombination: in the $\mathrm{H}\beta/\mathrm{H}\alpha$ ratio (panel a), the difference is small across the full parameter range. In the $\mathrm{H}\gamma/\mathrm{H}\beta$ ratio (panel b), however, recombination produces a visible deviation at $kT_e = 10$ eV for $n_e \gtrsim 10^{13}$ cm^{-3}, where the dashed 10 eV curve separates from its solid counterpart. Vinoth et al. omitted recombination from their model; the present results suggest this introduces error at the low-temperature, high-density boundary of their stated parameter range.

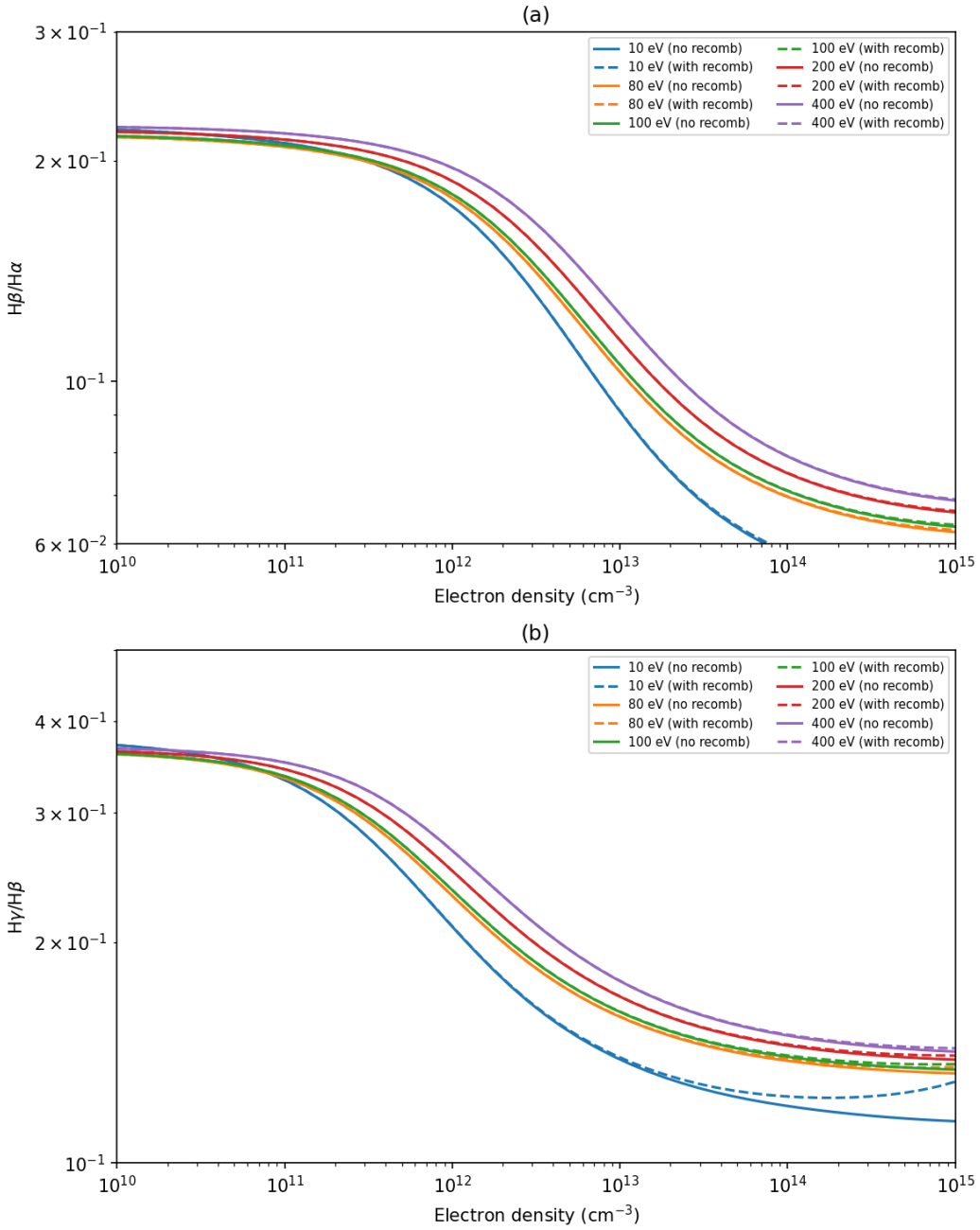

Figure 1: Hβ/Hα (a) and Hγ/Hβ (b) versus n_e at five temperatures. Solid lines: without recombination, reproducing Vinoth et al. [2]. Dashed lines: with three-body recombination included. The difference is most visible in Hγ/Hβ at 10 eV and $n_e \gtrsim 10^{13}$ cm^{-3}.

5.2 Steady-State Line Ratio Contours

Figure 2 shows an extension of the model beyond the analysis in Vinoth et al. into two dimensions to create contour maps of Hβ/Hα and Hγ/Hβ across the parameter space kT_e = 1–200 eV and $n_e = 10^{10}$–10^{15} cm^{-3}. At low density the contours are nearly vertical, indicating dependence on temperature only (coronal regime). As density increases through the collisional-radiative transition

($n_e \sim 10^{11}$–10^{13}), the ratios develop increased density sensitivity. At high temperature ($kT_e \gtrsim 10$ eV), both ratios flatten and become insensitive to further temperature increases.

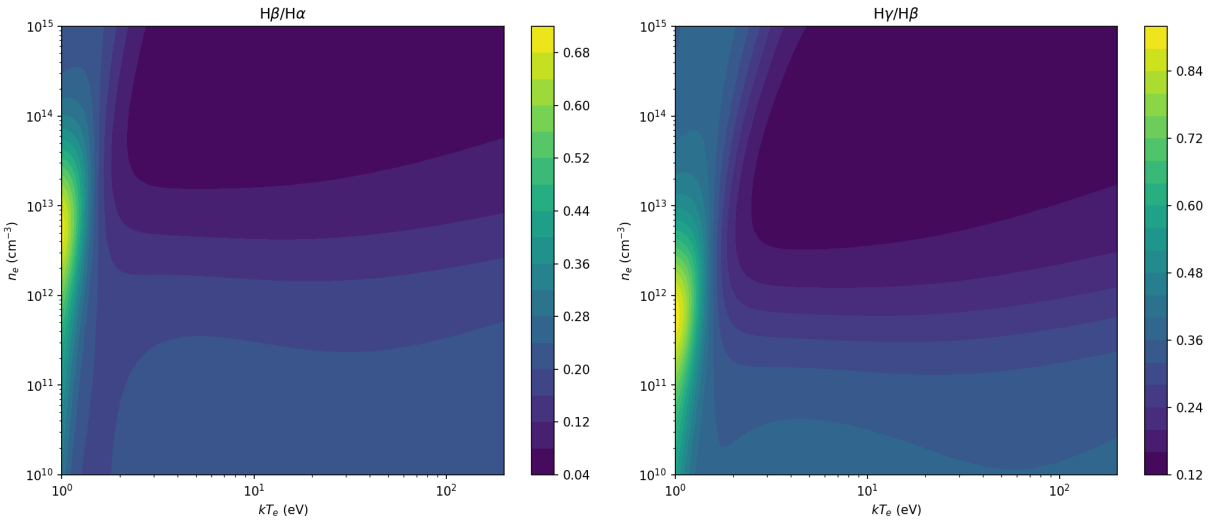

Figure 2: Contour maps of Hβ/Hα (left) and Hγ/Hβ (right) in the (kT_e, n_e) plane, computed with the full model including recombination.

5.3 Diagnostic Sensitivity Maps

Figure 3 shows the magnitude of the partial derivatives $|\partial(\text{ratio})/\partial \log T_e|$ and $|\partial(\text{ratio})/\partial \log n_e|$ across the parameter space. These maps quantify the diagnostic sensitivity: large gradients indicate regions where small changes in plasma parameters produce measurable changes in line ratios.

Temperature sensitivity (left column) is concentrated below $kT_e \sim 5$ eV. Above this threshold, the excitation energies for levels $n = 3$, 4, and 5 (12.1, 12.8, and 13.1 eV respectively) are all much larger than kT_e, and their Boltzmann factors saturate together, causing the ratio to flatten. Density sensitivity (right column) peaks in the collisional-radiative transition band $n_e \sim 10^{11}$–10^{13} cm^{-3}, where collisional and radiative rates are comparable. Below this band (coronal regime), n_e cancels out of the ratio entirely. Above it, populations begin approaching LTE and the density dependence again weakens.

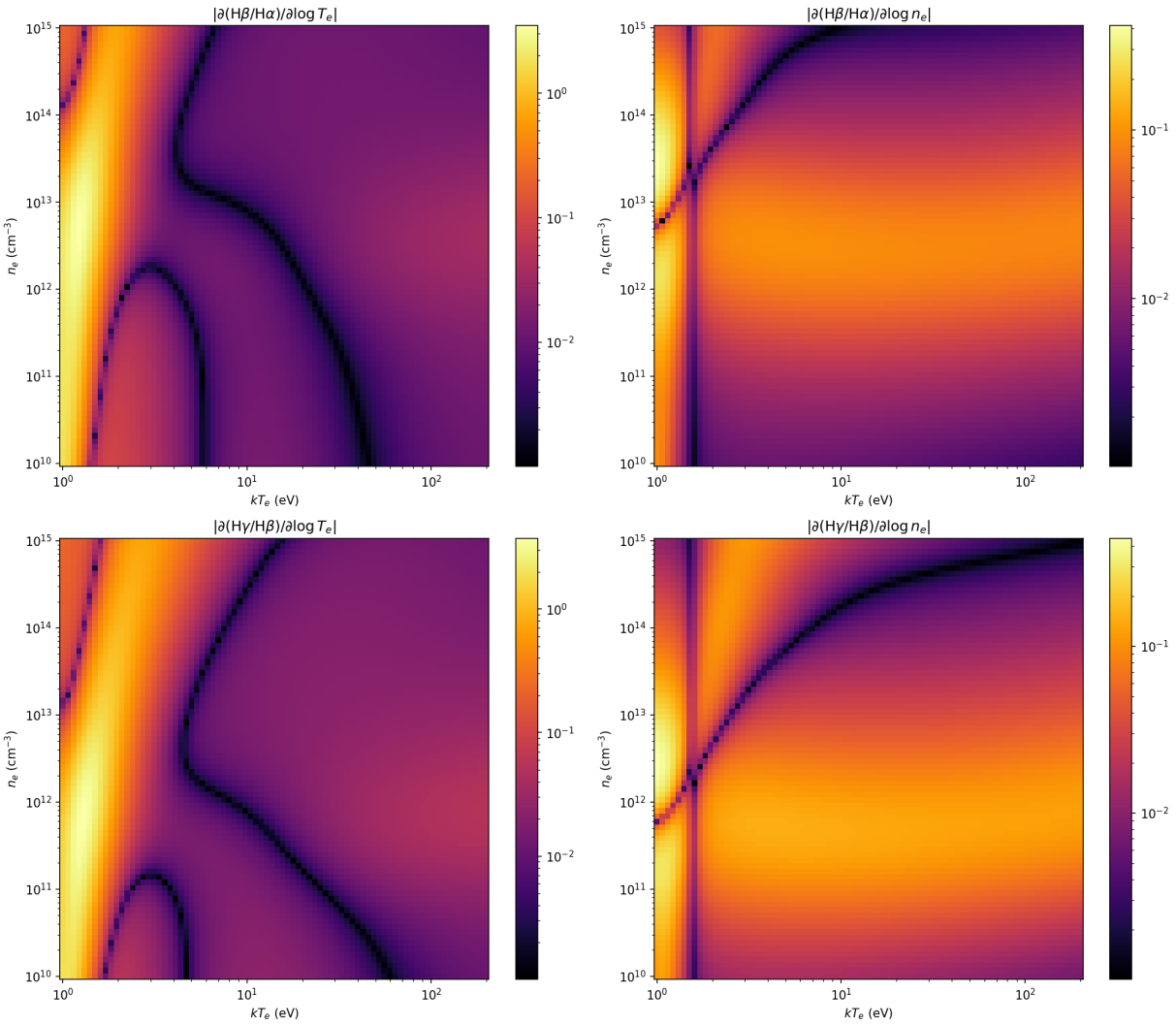

Figure 3: Sensitivity maps on a logarithmic color scale. Left column: $|\partial(\text{ratio})/\partial \log T_e|$. Right column: $|\partial(\text{ratio})/\partial \log n_e|$. Top row: H$\beta$/H$\alpha$. Bottom row: H$\gamma$/H$\beta$. Black curves mark zero-crossings where the gradient changes sign.

5.4 Time-Dependent Response

To assess when the steady-state assumption breaks down, the model was driven with a sinusoidally oscillating electron temperature in a sensitive area in the parameter space, $kT_e(t) = 5 + 3\sin(2\pi f t)$ eV, at fixed $n_e = 10^{12}$ cm^{-3}. The time-dependent Hβ/Hα ratio was compared to the instantaneous steady-state prediction at each moment.

At 1 kHz (Fig. 4a), the time-dependent and steady-state predictions overlap: the populations have ample time to equilibrate within each oscillation cycle. At 10 kHz (Fig. 4b), a difference emerges. At 100 kHz (Fig. 4c), the time-dependent response is significantly different from the steady-state prediction. The time-dependent amplitude is approximately three times larger than the steady-state prediction, and the waveform is strongly distorted. This amplification likely occurs because the populations transiently sample the high-sensitivity low-temperature regime during each

cycle and do not have time to relax back to the low-sensitivity steady state.

The fractional RMS diagnostic error, defined as the root-mean-square difference between the time-dependent and steady-state Balmer ratios normalized by the mean ratio, grows from 0.02% at 1 kHz to 2% at 100 kHz to 85% at 10 MHz.

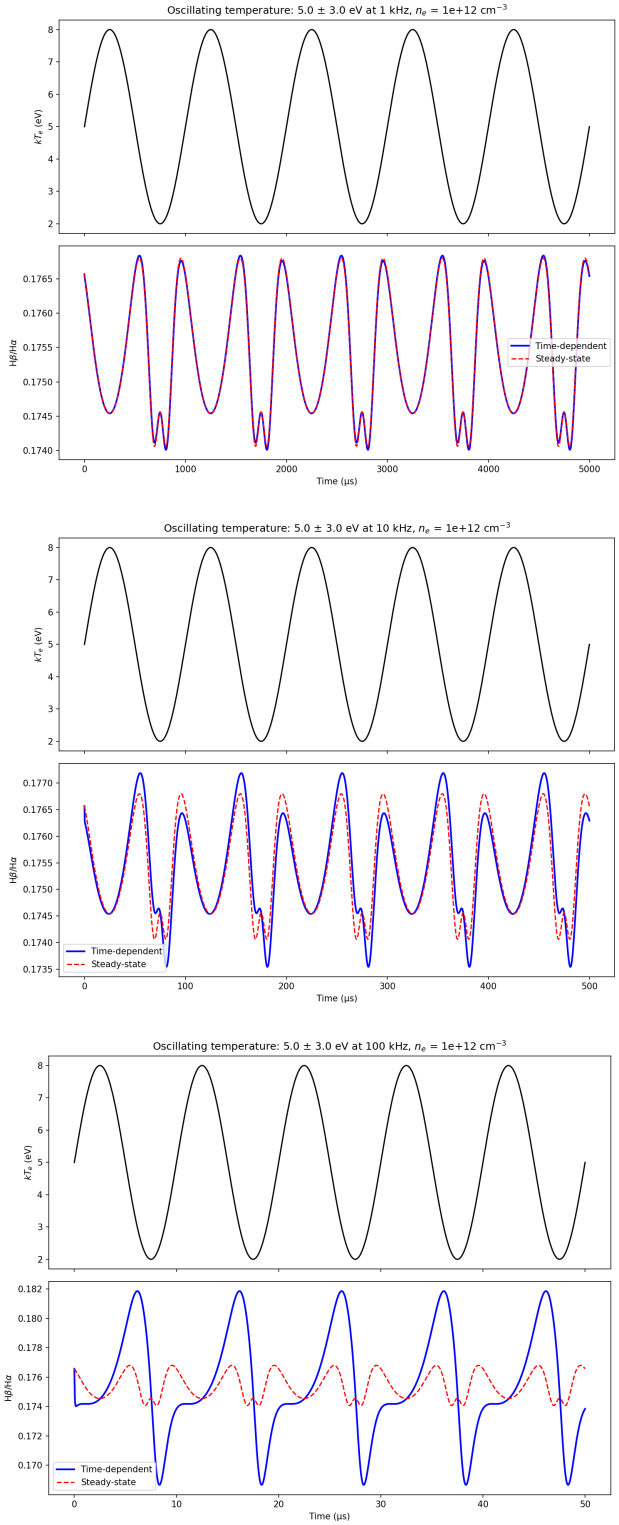

Figure 4: Time-dependent (blue solid) versus steady-state (red dashed) Hβ/Hα for sinusoidally oscillating temperature at $n_e = 10^{12}$ cm^{-3}. (a) 1 kHz: perfect tracking. (b) 10 kHz: partial tracking with some features missed. (c) 100 kHz: significant departure with nonlinear amplification.

To systematically map the diagnostic validity boundary, the fractional RMS error between the time-dependent and steady-state Balmer ratios was computed across a grid of oscillation frequencies and electron densities (Fig. 5). The black contour marks 5% error. At low frequency and high density (upper left), steady-state diagnostics are reliable (error $< 0.1\%$). At high frequency and low density (lower right), the error exceeds 100%. The 5% boundary runs roughly diagonally from $\sim$10 kHz at $n_e = 10^{10}$ cm^{-3} to $\sim$10 MHz at $n_e = 10^{15}$ cm^{-3}, reflecting the fact that higher density produces faster collisional equilibration.

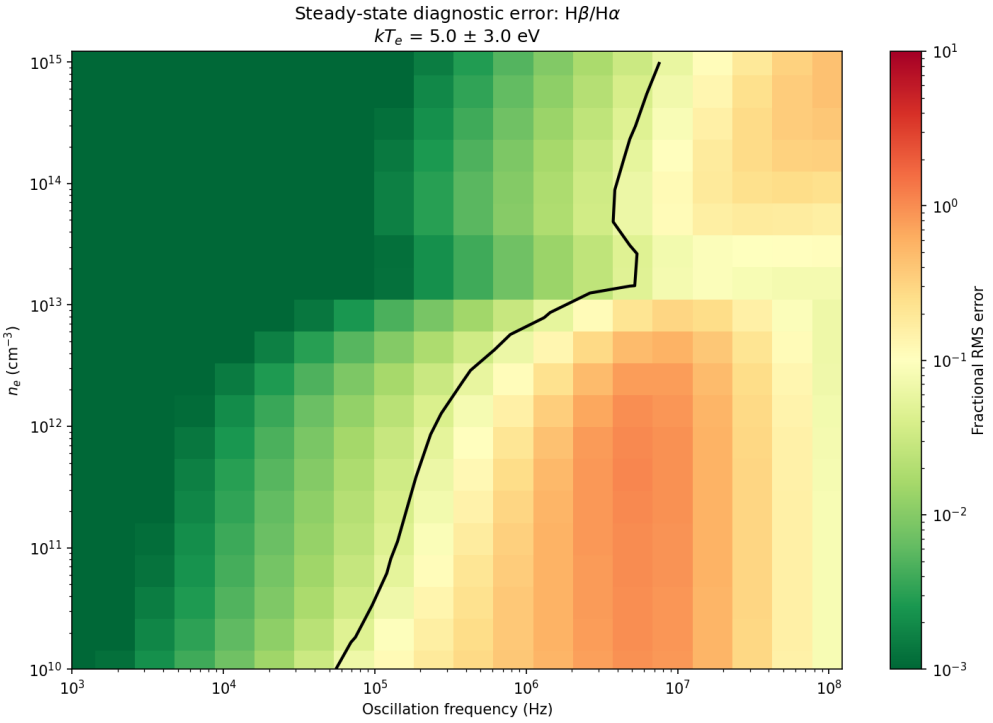

Figure 5: Fractional RMS diagnostic error across oscillation frequency and electron density for $kT_e = 5 \pm 3$ eV. Green: steady-state diagnostics are reliable. Red: steady-state prediction fails. Black contour: 5% error boundary.

5.5 Sources of Error and Reliability

The dominant source of uncertainty in the model is the Vriens and Smeets rate coefficients, which the authors estimate to be accurate to 10–20% for excitation and ionization rates [1]. The Johnson oscillator strengths introduce errors below 0.5% [3], and the Einstein A coefficients agree with exact quantum mechanical values to better than 0.1% (Table 2), so the atomic data contributes negligible error compared to the collisional rates.

To estimate the uncertainty in the Balmer ratios due to the 10–20% accuracy of the Vriens and Smeets rate coefficients, all collisional rates were scaled by $\pm 20\%$ while holding the Einstein A coefficients fixed. Table 1 shows the resulting spread in Hβ/Hα at representative points across the parameter space. The spread is at most $\sim$5%, confirming that the rate coefficient uncertainties do not qualitatively change the results.

The Vinoth comparison also provides external validation: the agreement in both shape and magnitude of the line ratio curves across five temperatures confirms that the implementation is

consistent with an independent CR model using the same underlying rate coefficients. A precise quantitative comparison was not performed because the Vinoth et al. results were compared visually rather than in a than digitized manner.

For the time-dependent results, the BDF integrator uses relative and absolute tolerances of 10^{-8} and 10^{-12} respectively, making numerical integration error negligible. The tracking contour grid uses 20×20 points; finer grids would smooth the contour boundary but not likely change its location significantly.

kT_e (eV)	n_e (cm^{-3})	Hβ/Hα (nominal)	Spread ($\pm$20%)
5.0	10^{10}	0.2220	$< 0.1\%$
5.0	10^{12}	0.1766	4.9%
10.0	10^{12}	0.1734	5.3%
10.0	10^{14}	0.0585	$< 0.1\%$
100.0	10^{12}	0.1800	4.4%

Table 1: Hβ/Hα uncertainty from $\pm$20% scaling of Vriens and Smeets collisional rate coefficients. The spread is largest in the collisional-radiative transition region where collisional and radiative rates compete.

6 Discussion

6.1 Where Are Balmer Diagnostics Useful?

The sensitivity maps provide a direct answer to the central question: Balmer line ratios are effective temperature diagnostics only below $kT_e \sim 5$ eV, and effective density diagnostics in the range $n_e \sim 10^{11}$–10^{13} cm^{-3}. Outside these windows, the gradients drop by one to two orders of magnitude, meaning that realistic measurement uncertainties of a few percent in the line ratio translate to unacceptably large uncertainties in the inferred plasma parameters. This is consistent with the qualitative observation of Vinoth et al. [2] that temperature determination becomes difficult at high T_e.

Choice of line ratio is also an important factor in diagnostics. Hγ/Hβ retains density sensitivity to slightly higher temperatures and lower densities than Hβ/Hα, suggesting that using both ratios together can extend the useful diagnostic range.

6.2 Recombination Effects

Comparing the model with and without recombination (Fig. 1) reveals that recombination produces visible shifts in the Balmer ratios at the low-temperature ($kT_e = 10$ eV), high-density ($n_e \gtrsim 10^{13}$ cm^{-3}) boundary of Vinoth et al.'s parameter range. While the higher-temperature curves are essentially unchanged, the 10 eV curve—the lowest temperature they consider—is affected. Furthermore, including recombination is also essential for validating the model against the LTE limit, which requires ionization-recombination balance.

6.3 When Does Steady-State Break Down?

The time-dependent extension shows that at $n_e = 10^{12}$ cm^{-3}, steady-state diagnostics are reliable for plasma variations slower than ∼10 kHz but fail above ∼100 kHz. This timescale is set by the

slowest eigenvalue of the rate matrix ($\tau \approx 90$ ns at this density), confirmed independently by the step-response simulations (Appendix B).

The amplification effect at 100 kHz is particularly important: the time-dependent Balmer ratio oscillates with three times the amplitude predicted by the steady-state model. A diagnostician using the steady-state model to interpret these oscillations would not only get the wrong phase but would dramatically underestimate the variation in the line ratio. This nonlinear amplification arises because the rate matrix $\mathbf{M}$ itself depends on temperature, so the system responds unevenly to temperature change—an effect not extractable from the linear eigenvalue analysis.

The tracking contour (Fig. 5) extends this analysis across the full (f, n_e) parameter space, showing that the critical frequency scales with density: at $n_e = 10^{10}$ cm^{-3} the 5% error boundary is near 10 kHz, while at $n_e = 10^{15}$ cm^{-3} it extends nearly to 10 MHz. This provides key information for diagnostics: given the density of a pulsed plasma, the contour directly indicates the maximum rate of variation for which steady-state spectroscopic diagnostics remain valid.

7 Conclusions

This model revealed a set of interesting dynamics in the diagnostic capabilities of Balmer line ratios across a wide range of electron temperatures and densities. The main findings are:

1. Balmer line ratios are sensitive temperature diagnostics only below $kT_e \sim 5$ eV, and sensitive density diagnostics only in the range $n_e \sim 10^{11}$–10^{13} cm^{-3}.

2. Three-body recombination produces measurable effects at the low-temperature, high-density edge of the parameter range studied by Vinoth et al., and is required for LTE validation. Its omission may introduce errors for plasmas near $kT_e \sim 10$ eV and $n_e \gtrsim 10^{13}$ cm^{-3}.

3. Steady-state spectroscopic diagnostics are reliable for plasma variations slower than ∼10 kHz at $n_e = 10^{12}$ cm^{-3}, with the critical frequency scaling with density through the eigenvalues of the rate matrix.

4. At higher frequencies, the time-dependent response exhibits nonlinear amplification that causes the steady-state model to underestimate diagnostic oscillations by up to a factor of three.

Future work could extend the model to include molecular hydrogen dissociation (which Vinoth et al. showed significantly affects line ratios) and an application to specific experimental scenarios with realistic plasma transients.

References

1. L. Vriens and A. H. M. Smeets, "Cross-section and rate formulas for electron-impact ionization, excitation, deexcitation, and total depopulation of excited atoms," *Phys. Rev. A* **22**, 940–951 (1980).

2. S. P. Vinoth, E. S. Evans, C. P. S. Swanson, E. Palmerduca, and S. A. Cohen, "Evaluation of a collisional radiative model for electron temperature determination in hydrogen plasma," *Rev. Sci. Instrum.* **93**, 093503 (2022).

3. L. C. Johnson, "Approximations for collisional and radiative transition rates in atomic hydrogen," *Astrophys. J.* **174**, 227–236 (1972).

4. V. B. Berestetskii, E. M. Lifshitz, and L. P. Pitaevskii, *Quantum Electrodynamics*, 2nd ed. (Pergamon, Oxford, 1982). Tabulated transition probabilities available at `https://www.ioffe.ru/astro/QC/CMBR/sp_tr.html`.

A Verification Tables

Transition	Computed (s^{-1})	Berestetskii (s^{-1})	Error
$2 \to 1$	4.697×10^8	4.697×10^8	$< 0.01\%$
$3 \to 2$	4.409×10^7	4.408×10^7	0.02%
$3 \to 1$	5.573×10^7	5.573×10^7	$< 0.01\%$
$4 \to 2$	8.416×10^6	8.416×10^6	$< 0.01\%$

Table 2: Einstein A coefficients compared to exact quantum mechanical values from Berestetskii et al. [4].

N_{levels}	Hβ/Hα	Hγ/Hβ
10	0.1777	0.2310
12	0.1750	0.2176
15	0.1733	0.2099
18	0.1727	0.2072

Table 3: Convergence of Balmer ratios with number of atomic levels at $kT_e = 10$ eV, $n_e = 10^{12}$ cm^{-3}.

B Step Response and Eigenvalue Validation

Figure 6 shows the Balmer ratio response to a step change in temperature from 10 to 50 eV at three densities. The green dotted lines mark the slowest eigenvalue timescale $\tau = -1/\lambda_{\min}$ at each density. The eigenvalue prediction correctly identifies the order of magnitude of the equilibration time: $\tau = 3.0$ μs at $n_e = 10^{10}$, $\tau = 90$ ns at $n_e = 10^{12}$, and $\tau = 2.5$ ns at $n_e = 10^{14}$ cm^{-3}.

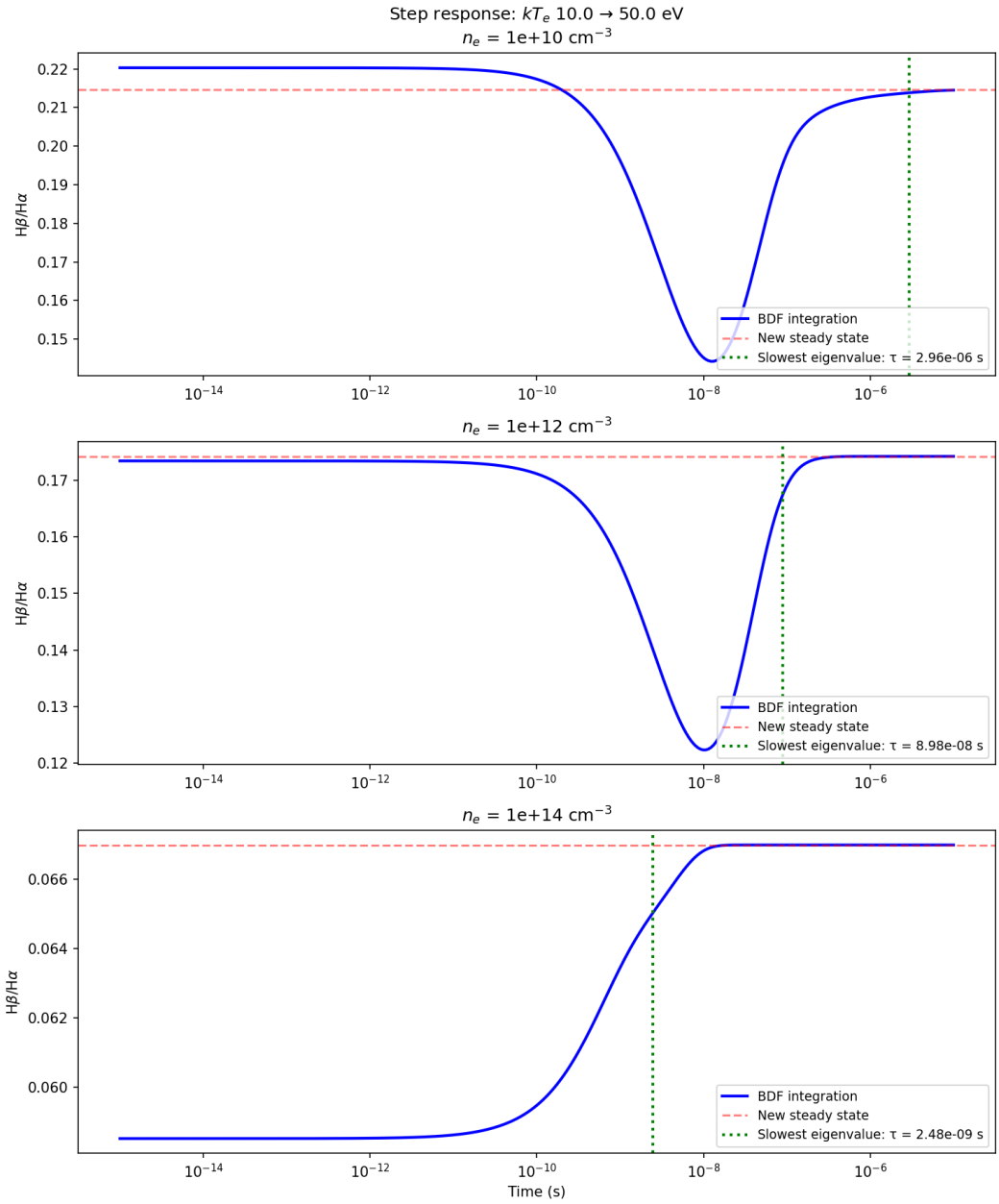

Figure 6: Hβ/Hα response to a step change kT_e: 10 $\rightarrow$ 50 eV at three electron densities. Green dotted lines: slowest eigenvalue prediction.